

Side-band Inequivalence: The Unexpected Symmetry Breaking

Sina Khorasani*
(Dated: January 15, 2019)

In this letter, the recently predicted Side-band Inequivalence in quantum optomechanics is analyzed to the full order. It is shown that not only frequency shifts due to blue- and red-scattered (Stokes and anti-Stokes) mechanical side-bands are counter-intuitively unequal, but also there exists a maximum attainable side-band inequivalence which may be expected at an optimal operation point. The mathematical method employed here is a combination of operator algebra equipped with harmonic balance, which allows a clear understanding of the associated nonlinear process. This reveals the existence of three distinct operation regimes in terms of pump power or intracavity photon number, two of which have immeasurably small side-band inequivalence. Compelling evidence from Raman scattering data of various materials unambiguously confirms existence of a previously unnoticed side-band inequivalence.

PACS numbers: 42.50.-p, 42.50.Lc, 42.65.Dr

The nonlinearity of optomechanical interaction [1–9] causes scattering of incident photons with the annihilator \hat{a} from the cavity unto either red- or blue-shifted photons through annihilation or generation of a cavity phonon with the annihilator \hat{b} , giving rise to the first-order mechanical side-bands. Taking the optical frequency ω to be at a detuning $\Delta = \omega_c - \omega$ from cavity resonance ω_c , the ν -th order sidebands are naturally expected to occur at the detunings $\Delta_{\pm\nu} = \Delta \mp \nu\Omega$, where Ω represents the mechanical frequency. As a result, the first-order mechanical side-bands of scattered red Δ_{+1} and blue Δ_{-1} processes must average out back to the original pump detuning Δ .

Defining the side-band inequivalence as the deviation of this average from Δ , as $\delta = \frac{1}{2}(\Delta_{+1} + \Delta_{-1}) - \Delta$, then one may conclude $\delta = 0$. A non-zero δ would have otherwise implied the so-called Side-band Inequivalence. This type of asymmetry appears to have a classical nonlinear nature, and is illustrated in Fig. 1.

There is, however, another well-known type of side-band asymmetry between the red and blue side-bands in the context of optomechanics, which has a quantum nature and may be used for instance to accurately determine the absolute temperature through a reference-free optomechanical measurement [10, 11]. This is based on the ratio of Stokes to anti-Stokes Raman transition rates, which is equal to $\exp(\hbar\Omega/k_B T)$ where k_B is the Boltzmann's constant and T is the absolute temperature [12, 13]. Clearly, side-band inequivalence is quite different from this type of side-band asymmetry.

While both time-reversal symmetry and energy conservation are fundamentally preserved in this scattering process, a nonlinear analysis of quantum optomechanics using the recently developed method of higher-order operators [14–18] necessitates a slight difference among detunings of blue and red-scattered photons, the amount of which was initially found to increase roughly proportional to the intracavity photon number \bar{n} . Here, \bar{n} is defined as the steady-state mean-value of the number operator

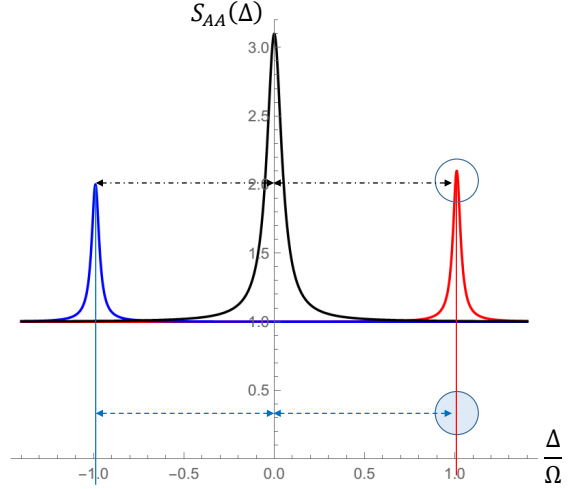


FIG. 1. Illustration of two basic symmetry breakings in quantum optomechanical cavity at resonant pump, and in absence of cooling tone: (a) Side-band Inequivalence – The red detuning exceeds that of blue detuning, shown in blue dashed arrows; (b) Side-band Asymmetry – The red peak exceeds that of blue peak, shown in black dash-dotted arrows. Here, $S_{AA}(\Delta)$ represents the spectral noise density.

$$\hat{n} = \hat{a}^\dagger \hat{a}.$$

Surprisingly enough, this disagreement satisfying $\delta \neq 0$ does not violate the energy conservation law, actually allowed by the finite cavity linewidth as well as the single-photon/single-phonon nature of the process involved. Moreover, the time-reversal symmetry is also preserved.

Among the pool of available experimental data, only a handful of side-band resolved cavities reveal this disagreement [14]. Some initial trial experiments recently done at extremely high intracavity photon numbers \bar{n} , and/or extremely large single-photon optomechanical interaction rates g_0 , though, failed to demonstrate its existence. This may raise the speculation that whether side-band inequivalence would have been merely a mathematical artifact, or something has been missing due to not doing the operator analysis to the highest-order.

A careful analysis of this phenomenon, however, con-

firms the latter, thus classifying the quantum optomechanical interaction into three distinct regimes with different behaviors:

- **Fully Linear:** This regime can be investigated using the lowest-order analysis and first-order operators, which is conventionally done by linearizing the Hamiltonian around equilibrium points. This will require the four-dimensional basis of first-order ladder operators $\{\hat{a}, \hat{a}^\dagger, \hat{b}, \hat{b}^\dagger\}$ and is indeed quite sufficient to understand many of the complex quantum optomechanical phenomena [19].
- **Weakly Nonlinear:** This regime requires higher-order operator analysis of at least second-order. This can be done using the three-dimensional reduced basis [14, 19] given as $\{\hat{a}, \hat{a}\hat{b}, \hat{a}\hat{b}^\dagger\}$.
- **Strongly Nonlinear:** Full understanding of this interaction regime requires the highest-order analysis using third-order operators. Referred as to the minimal basis [14, 19], the convenient reduced choice is the two-dimensional basis $\{\hat{n}^2, \hat{n}\hat{b}\}$. While most of the quantum optomechanical experiments happen to fall in this regime, the striking behavior of governing equations is in such a way that a fully-linearized analysis of fluctuations mostly happens to work.

Side-band Inequivalence is essentially forbidden in the fully linear regime, and it also quickly fades away in the strongly nonlinear regime. But it may only happen in the weakly nonlinear regime. This is now also confirmed both by the higher-order operator method and extensive calculations. It typically does not exceed one part in million to one part in ten thousand, and therefore, it is a very delicate phenomenon and elusive to observe.

This letter provides a direct route towards clear understanding of this complex nonlinear phenomenon. Using a combination of operator algebra and harmonic balance (used in analysis of laser diodes) [20], we obtain a closed form expression for side-band inequivalence δ as a function of intracavity photon number \bar{n} , which is expected to be valid through all three above operation regimes, and for any arbitrarily chosen set of optomechanical parameters. It can be shown that there is an optimal point at which the side-band inequivalence attains a maximum. Moving away from the optimal point, both at the much smaller and much larger pump rates, δ attains much smaller values, tending to zero in the limit of very large \bar{n} .

This will be greatly helpful to designate the investigation range of experimental parameters given any available optomechanical cavity. Furthermore, it marks a clear and definable border among the three above-mentioned operation regimes.

The analysis of side-band inequivalence proceeds with considering the behavior of optomechanical cavity under steady-state conditions. We will focus only on the first-order side-bands and discard all other contributions com-

ing from or to the second- and higher-order side-bands. We consider a single-frequency pump with ideally zero linewidth at a given detuning Δ , which normally gives rise to two stable blue- and red- side-bands. Hence, the time-dependence of the photon annihilator will look like

$$\hat{a}(t) = \hat{a}_0 e^{i\Delta t} + \hat{a}_b e^{i(\Delta - \Omega + \frac{1}{2}\delta)t} + \hat{a}_r e^{i(\Delta + \Omega + \frac{1}{2}\delta)t} + \dots, \quad (1)$$

where \hat{a}_0 , \hat{a}_b , and \hat{a}_r respectively correspond to the central excitation resonance at pump frequency, and blue- and red-detuned side-bands. The steady-state time-average of central excitation satisfies $\langle \hat{a}_0 \rangle = \sqrt{\bar{n}}$, where \bar{n} can be determined by solution of a third-order algebraic equation once the optical power pump rate P_{op} , detuning Δ , external coupling η and all other optomechanical parameters are known. The standard set of basic optomechanical parameters needed here are mechanical frequency Ω , optical decay rate κ , and mechanical decay rate Γ . Therefore, the photon number operator will behave as

$$\begin{aligned} \hat{n}(t) = & \hat{a}_0^\dagger \hat{a}_0 + \hat{a}_b^\dagger \hat{a}_b + \hat{a}_r^\dagger \hat{a}_r \\ & + \hat{a}_b^\dagger \hat{a}_0 e^{i(-\Omega + \frac{1}{2}\delta)t} + \hat{a}_0 \hat{a}_b^\dagger e^{-i(-\Omega + \frac{1}{2}\delta)t} + \\ & + \hat{a}_r^\dagger \hat{a}_0 e^{i(\Omega + \frac{1}{2}\delta)t} + \hat{a}_0 \hat{a}_r^\dagger e^{-i(\Omega + \frac{1}{2}\delta)t} + \dots, \end{aligned} \quad (2)$$

while the mechanical annihilator will exhibit a closely spaced doublet around the mechanical frequency spaced within δ as

$$\hat{b}(t) = \hat{b}_0 + \hat{b}_b e^{-i(\Omega - \frac{1}{2}\delta)t} + \hat{b}_r e^{-i(\Omega + \frac{1}{2}\delta)t} + \dots. \quad (3)$$

Here, the average mechanical displacement satisfies

$$b_0 = \langle \hat{b}_0 \rangle = \frac{ig_0 \bar{n}}{i\Omega + \frac{1}{2}\Gamma}. \quad (4)$$

Now, let us get back to the Langevin equation for mechanical motions, which simply is

$$\frac{d}{dt} \hat{b}(t) = (-i\Omega - \frac{1}{2}\Gamma) \hat{b}(t) + ig_0 \hat{n}(t) + \sqrt{\Gamma} \hat{b}_{\text{in}}(t), \quad (5)$$

where $\hat{b}_{\text{in}}(t)$ is the operator for mechanical fluctuations. For the purpose of our analysis here, all fluctuations can be discarded since they are irrelevant to the formation of side-band frequencies and average out to zero. Using (2) and (3) we get

$$\begin{aligned} & -i(\Omega + \frac{\delta}{2}) \hat{b}_r e^{-i(\Omega + \frac{\delta}{2})t} - i(\Omega - \frac{\delta}{2}) \hat{b}_b - b e^{-i(\Omega - \frac{\delta}{2})t} \\ & \approx -(i\Omega + \frac{\Gamma}{2}) \hat{b}_r e^{-i(\Omega + \frac{\delta}{2})t} - (i\Omega + \frac{\Gamma}{2}) \hat{b}_b e^{-i(\Omega - \frac{\delta}{2})t} \\ & + ig_0 \hat{a}_0 \hat{a}_b e^{-i(\Omega - \frac{\delta}{2})t} + ig_0 \hat{a}_r^\dagger \hat{a}_0 e^{-i(\Omega + \frac{\delta}{2})t} + \dots. \end{aligned} \quad (6)$$

From the above, we obtain two key operator equations

$$\begin{aligned} \hat{b}_r &= \frac{i2g_0}{-i\delta + \Gamma} \hat{a}_r^\dagger \hat{a}_0, \\ \hat{b}_b &= \frac{i2g_0}{i\delta + \Gamma} \hat{a}_0 \hat{a}_b. \end{aligned} \quad (7)$$

In a similar manner, the Langevin equation for the photon annihilator is

$$\frac{d}{dt}\hat{a}(t) = (i\Delta - \frac{1}{2}\kappa)\hat{a}(t) + ig_0\hat{a}(t)[\hat{b}(t) + \hat{b}^\dagger(t)] + \sqrt{\kappa}\hat{a}_{\text{in}}. \quad (8)$$

Using (1) and (3) we obtain

$$\begin{aligned} & i\Delta\hat{a}_0e^{i\Delta t} + i(\Delta - \Omega + \frac{\delta}{2})\hat{a}_be^{i(\Delta - \Omega + \frac{\delta}{2})t} \\ & + i(\Delta + \Omega + \frac{\delta}{2})\hat{a}_re^{i(\Delta + \Omega + \frac{\delta}{2})t} \approx \\ & (i\Delta - \frac{\kappa}{2}) \left[\hat{a}_0e^{i\Delta t} + \hat{a}_be^{i(\Delta - \Omega + \frac{\delta}{2})t} + \hat{a}_re^{i(\Delta + \Omega + \frac{\delta}{2})t} \right] \\ & + ig_0 \left[\hat{a}_0e^{i\Delta t} + \hat{a}_be^{i(\Delta - \Omega + \frac{\delta}{2})t} + \hat{a}_re^{i(\Delta + \Omega + \frac{\delta}{2})t} \right] \times \\ & \left[\hat{b}_0 + \hat{b}_0^\dagger + \hat{b}_re^{-i(\Omega + \frac{\delta}{2})t} + \hat{b}_be^{-i(\Omega - \frac{\delta}{2})t} + \hat{b}_r^\dagger e^{i(\Omega + \frac{\delta}{2})t} + \hat{b}_b^\dagger e^{i(\Omega - \frac{\delta}{2})t} \right]. \end{aligned} \quad (9)$$

This will yield the further operator equations as

$$\begin{aligned} \frac{\kappa}{2ig_0}\hat{a}_0 &= \hat{a}_0(\hat{b}_0 + \hat{b}_0^\dagger) + \hat{a}_b\hat{b}_r^\dagger + \hat{a}_r\hat{b}_r, \quad (10) \\ \left[\frac{i(-\Omega + \frac{\delta}{2}) + \frac{\kappa}{2}}{ig_0} \right] \hat{a}_b &= \hat{a}_b(\hat{b}_0 + \hat{b}_0^\dagger) + \hat{a}_0\hat{b}_b, \\ \left[\frac{i(\Omega + \frac{\delta}{2}) + \frac{\kappa}{2}}{ig_0} \right] \hat{a}_r &= \hat{a}_r(\hat{b}_0 + \hat{b}_0^\dagger) + \hat{a}_0\hat{b}_r^\dagger. \end{aligned}$$

Now, substituting whatever we have in hand in the second equation of (10), and taking expectation values at the end, we obtain a key algebraic equation in terms of δ as

$$\begin{aligned} i \left(-\Omega + \frac{1}{2}\delta \right) + \frac{1}{2}\kappa &= ig_0(b_0 + b_0^*) \quad (11) \\ &+ ig_0\sqrt{\bar{n}} \frac{2ig_0\sqrt{\bar{n}}}{i\delta + \Gamma}. \end{aligned}$$

Rearrangement of the above gives rise to the equation

$$\begin{aligned} \delta^2 + [-i2\Omega + \gamma + 2g_0x_0]\delta \quad (12) \\ + [(2\Omega - i\kappa)\Gamma - 4g_0^2\bar{n} + 2i\Gamma g_0x_0] &= 0, \end{aligned}$$

in which $x_0 = b_0 + b_0^*$ and $\gamma = \kappa + \Gamma$ is the total optomechanical decay rate [14, 16].

This approximate nature of this equation will yield complex values for δ the imaginary value of which has to be discarded. Furthermore, it leaves room to ignore the the square terms δ^2 , to admit the solution

$$\delta = \Re \left[\frac{(2\Omega - i\kappa)\Gamma - 4g_0^2\bar{n} + 2i\Gamma g_0x_0}{\gamma - 2i\Omega + 2g_0x_0} \right]. \quad (13)$$

This solution can be put into the more convenient form using (4) and further simplification as

$$\begin{aligned} \delta(\bar{n}) &= \Re \left[\frac{A + B\bar{n}}{C - iD\bar{n}} \right] \quad (14) \\ &= \frac{\Re[AC^*] + (B\Re[C] + \Im[A]D)\bar{n}}{|C|^2 - 2\Im[C]D\bar{n} + D^2\bar{n}^2} \\ &= \frac{[2\Gamma\Omega(\kappa + \gamma)] + (B\gamma - \kappa\Gamma D)\bar{n}}{|C|^2 - 4\Omega D\bar{n} + D^2\bar{n}^2}, \end{aligned}$$

where

$$\begin{aligned} A &= \Gamma(2\Omega - i\kappa), \quad (15) \\ B &= \frac{4g_0^2(\Omega - \frac{1}{2}\Gamma)^2}{\Omega^2 + \frac{1}{4}\Gamma^2} = B^*, \\ C &= \gamma - 2i\Omega, \\ D &= \frac{4g_0^2\Omega}{\Omega^2 + \frac{1}{4}\Gamma^2} = D^*. \end{aligned}$$

The expression (14) obtained for the side-band inequivalence has interesting properties at the limits of zero and infinite intracavity photon number. We may obtain here after some simplification easily the limiting expressions

$$\lim_{\bar{n} \rightarrow \infty} \delta(\bar{n}) = 0, \quad (16)$$

$$\lim_{\bar{n} \rightarrow 0} \delta(\bar{n}) = \frac{2\Gamma\theta\Omega}{4\Omega^2 + \gamma^2} \approx 0,$$

with $\theta = \kappa + \gamma$, while noting that $\Gamma \ll \Omega$ and also for a side-band resolved cavity $\kappa \ll \Omega$, together which we have $\kappa < \gamma < \theta \ll \Omega$.

One should take into account the fact that for Doppler cavities, side-bands normally resolve well enough for a decisive measurement [19], and the concept of side-band inequivalence is only practically meaningful for side-band resolved cavities. Therefore, the following approximations are valid

$$A \approx 2\Gamma\Omega, \quad (17)$$

$$B \approx 4g_0^2,$$

$$C \approx -2i\Omega,$$

$$D \approx \frac{4g_0^2}{\Omega},$$

$$\begin{aligned} \delta(\bar{n}) &\approx \frac{\frac{1}{2}\Gamma\Omega^3\theta + g_0^2\Omega(\gamma\Omega - \kappa\Gamma)\bar{n}}{\gamma^2 + (\Omega^2 - 2g_0^2\bar{n})^2} \\ &\approx \frac{\frac{1}{2}\Gamma\Omega^3\theta + g_0^2\gamma\Omega\bar{n}}{\gamma^2 + (\Omega^2 - 2g_0^2\bar{n})^2}. \end{aligned}$$

As long as satisfies $\bar{n} \ll 2|\Im[C]|/D = \Omega^2/g_0^2$, then second order term \bar{n}^2 in the denominator of (15) is negligible and can be ignored. Under this regime, the side-band inequivalence varies almost linearly with \bar{n} as

$$\begin{aligned} \delta(\bar{n}) &\approx \frac{2\Gamma\theta\Omega}{4\Omega^2 + \gamma^2} + \frac{(B\gamma - \kappa\Gamma D)|C|^2 + 8\Omega^2\Gamma\theta D}{|C|^4}\bar{n} \\ &\approx \frac{g_0^2\gamma}{\Omega^2}\bar{n}. \quad (18) \end{aligned}$$

This result also behaves well in reasonable agreement with the expression obtained earlier for the side-band inequivalence [14] given as $\delta \approx g_0^2/\Omega$. The difference is within a fraction given by $\gamma/\Omega < 1$ which is typically less than unity.

The first immediate conclusion which can be obtained from (18) is that the side-band inequivalence δ is always

positive, meaning that the detuning frequency of red-sideband should be always a bit larger in magnitude than the blue-sideband. This also agrees with the previous findings of higher-order operator algebra [14].

Another very important result which can be drawn from the above discussions, is marking the boundaries of linear, weakly nonlinear, and strongly nonlinear interaction regimes in quantum optomechanics. This follows by normalizing δ with respect to the mechanical frequency Ω first.

The linear regime is easily given by $\bar{n} < \Omega^2/g_0^2$, where intracavity photon number is essentially too low to cause any appreciable side-band inequivalence.

The weakly nonlinear regimes is next given by $\Omega^2/g_0^2 < \bar{n} < \Omega^3/g_0^2\gamma$, where the side-band inequivalence increases almost linearly.

The strongly nonlinear regime at larger intracavity photon numbers satisfying $\bar{n} > \Omega^3/g_0^2\gamma$ will push the system into strongly nonlinear regime where the side-band inequivalence quickly start to fade away.

The unique mathematical form of (14) which is composed of a first- and second-order polynomials in terms of \bar{n} respectively, offers a clear maximum at a certain optimum intracavity photon number \bar{n}_{\max} . To do this, let us first define the dimensionless constants $\alpha = 2g_0^2\gamma/\Gamma\Omega\theta$ and $\beta = 2g_0^2/\Omega^2$, $\vartheta = \gamma/\Omega$, and $\psi = \Gamma\theta/2\Omega^2$. Then, the side-band inequivalence (17) can be rewritten as

$$\delta(\bar{n}) = \Omega\psi \frac{1 + \alpha\bar{n}}{\vartheta^2 + (1 - \beta\bar{n})^2}. \quad (19)$$

This offers the optimum intracavity photon number as

$$\bar{n}_{\max} = \frac{\sqrt{(\alpha + \beta)^2 + \alpha^2\vartheta}}{\alpha\beta} - \frac{1}{\alpha} \approx \frac{1}{\beta} = \frac{\Omega^2}{2g_0^2}, \quad (20)$$

and thus the maximum attainable side-band inequivalence as

$$\delta_{\max} = \delta(\bar{n}_{\max}) \approx \Omega\psi \frac{\alpha\beta}{\vartheta} = \frac{2g_0^4}{\Omega^3}. \quad (21)$$

Some further simplification and noting the fact that $\Omega \gg \Gamma\theta/\gamma$ or $\alpha \gg \beta$ and $\vartheta \ll 1$, we conclude that the maximum practically measurable side-band inequivalence must be simply given by $\delta_{\max} = 2g_0^4/\Omega^3$ at the optimum intracavity photon number $\bar{n}_{\max} = \Omega^2/2g_0^2$. This should fall at the onset of weakly nonlinear regime. In Fig. 2, variation of side-band inequivalence versus intracavity photon number and in terms of different settings for input parameters $\{\alpha, \beta, \vartheta\}$ is illustrated.

It is easy to verify that the side-band inequivalence does not violate the two fundamental symmetries of the nature. Here, both the time-reversal symmetry as well as the conservation of energy are preserved. The energy of scattered red- and blue- photons $\hbar\omega \mp \hbar\Omega$ is normally expected to be within the energy of one phonon $\hbar\Omega$ where ω

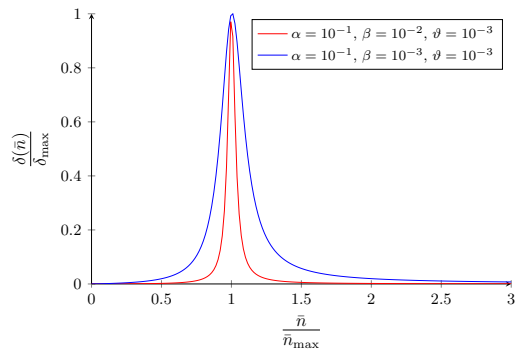


FIG. 2. Variation of side-band inequivalence around the maximum point in terms of various settings of parameters.

is the angular frequency of incident electromagnetic radiation. Per every annihilated photon, exactly one phonon is either annihilated, giving rise to a blue-shifted photon, or one phonon is created, giving rise to a red-shifted photon.

However, not all photons and not all phonons are having exactly the same energies. This is permissible by the non-vanishing mechanical $\Gamma > 0$ and optical linewidths $\kappa > 0$ of the cavity. One should expect that once these two quantities vanish, the side-band inequivalence is gone. This expectation is actually correct, and is met by the relation for the maximum observable side-band inequivalence δ_{\max} . Hence, basically it should be not contradictory to have a possible non-zero side-band inequivalence.

With regard to the time-reversal symmetry, one must take notice of the fact that all optical frequencies are physically positive, since we first must move back out of the rotating reference frame. For instance, the blue- and red-scattered photons have frequencies given by $\omega_b = \omega_c + \Omega - \frac{1}{2}\delta$ and $\omega_r = \omega_c - \Omega - \frac{1}{2}\delta$. Therefore, blue and red processes are not time-reversed processes of each other, as they both stay on the positive frequency axis. Negative frequency images corresponding to both processes do however exist and exactly satisfy the time-reversal.

Remarkably, the Stokes and anti-Stokes peaks of Raman spectra also exhibit the same phenomenon of side-band inequivalence. This has so far skipped the attention since normally the nonlinear interaction rate causing the formation of Raman scattering is too small for majority of bulk materials and liquids. Again, a full linear theory of Raman scattering [21] disallows side-band inequivalence. However, with the recent advent of low-dimensional materials, optical nonlinear interactions leading to Raman scattering [22, 25, 26, 31] and Kerr effect [27] are available at much stronger rates.

Table I provides a summary of measurable side-band inequivalence based on the reported Raman scattering of different materials. Calculations of normalized side-band inequivalence and errors are done according to the

best possible resolution of measurement graphs. It has to be noted that for every given material, the side-band inequivalence is a strong function of scattering order, excitation wavelength, polarization, angle of incidence, as well as intensity. Therefore, it is not possible to reconstruct a fit to varying function for δ as 19. However, the existence of a previously unnoticed side-band inequivalence, which is always leaning toward the red side-band seems to be conclusive. Therefore, a rigorous quantum theory of side-band inequivalence for Raman scattering from continuum optomechanics is yet to be developed, such as the one recently developed for materials [21].

TABLE I. Side-band inequivalence in Raman spectra of various materials, computed based on the highest-resolution available measurements. The last two rows are obtained by direct calculation on publicly available measurement data. Confidence interval for these two last measurements is remarkably significant, leaving no doubt in existence of side-band inequivalence.

Material	Side-band Inequivalence	Remarks
MoTe ₂	7% \pm 0.8%	6-layer [28]
MoS ₂	0.3% \pm 0.1%	6-layer [29]
CNT ^a	0.78% \pm 0.15%	flake [30]
	0.6% \pm 0.21%	(10, 5) SC ^b [23]
	0.2% \pm 0.1%	1st-order; SC ^b [24]
Gr ^c	1.22% \pm 0.13%	2nd-order; SC ^b [24]
	0.8% \pm 0.16%	4-layer [32]
	0.5% \pm 0.17%	3-layer [32]
S ^d	1.03% \pm 0.25%	1st-order; grains [30]
	0.72% \pm 0.18%	1st-order; grains [30]
	0.72% \pm 0.18%	1st-order; grains [30]
Ethanol	0.18% \pm 0.04%	1st-order; EX ^e [33]
B4 ^g	0.34% ^h \pm 0.018%	1090nm line [34, 35]
SRA ^f	0.1424% \pm 0.001%	Yb-doped fiber [36, 37]

^a CNT: Carbon Nano-tube

^b SC: Semiconducting

^c Gr: Graphene

^d S: Sulphur

^e EX: Excitation at 532nm

^g B4: Single Biphenyl-4-thiol molecule in monolayer confined to optical picocavity

^h 4-point moving average applied. Guassian 10-point filtering results in the much larger value of 1.06%.

^f SRA: Stimulated Raman Amplifier

Finally, it is easy to see that the same nonlinear symmetry breaking can lead to asymmetry in the particle pair production or parametric down conversion, which can be considered as the dual of optomechanical process [38, 39]. In order to observe this fact, consider an optomechanical system with a mechanical frequency roughly double the optical frequency $\Omega \approx 2\omega$. If the mechanics is driven strong enough at the frequency Ω , then the effective interaction Hamiltonian will be simply $\mathbb{H}_{\text{eff}} = i\hbar g(\hat{a}^\dagger \hat{a}^\dagger \hat{b} - \hat{a} \hat{a} \hat{b}^\dagger)$, where a phonon with energy $\hbar\Omega$ dissociates into two photons with energies $\hbar(\omega \pm \delta)$ with

δ representing the corresponding symmetry breaking in pair frequencies caused by side-band inequivalence.

Also, based on the duality of effective interaction Hamiltonian in linear electro-optic modulation (within the validity of rotating wave approximation), with the optomechanical Hamiltonian [40–42], one could predict that the same nonlinear inequivalence to appear in relevant experiments, too. Similar arguments should be valid for enhanced Raman scattering of single molecules by localized plasmonic resonances as well [43].

We presented a complete analysis of side-band inequivalence in quantum optomechanics, and showed it undergoes a maximum and obtained closed-form expressions for optimum intracavity photon number as well as maximum attainable side-band inequivalence. We classified the operation into the linear, weakly nonlinear, and strongly nonlinear regimes, in which the behavior of system is markedly different. The results of this investigation can provide the accuracy constraints as well as necessary experimental set up to resolve the elusive side-band inequivalence. Analysis of high resolution measurements of Raman scattering for different materials confirms the existence of side-band inequivalence. One could speculate that precise measurement of the variation of side-band inequivalence in terms of various system parameters could provide further insight into unexplored nonlinear properties of different material.

This article is dedicated to the celebrated artist, Anastasia Huppmann.

* sina.khorasani@ieee.org

- [1] Aspelmeyer M, Kippenberg T J and Marquardt F 2014 *Rev. Mod. Phys.* **86** 1391
- [2] Kippenberg T J and Vahala K J 2008 *Science* **321** 1172
- [3] Aspelmeyer M, Kippenberg T and Marquardt F 2014 *Cavity Optomechanics: Nano- and Micromechanical Resonators Interacting with Light* (Springer: Berlin)
- [4] Meystre P 2013 *Ann. Phys.* **525** 215
- [5] Bowen W P and Milburn G J 2016 *Quantum Optomechanics* (CRC Press: Boca Raton)
- [6] Gu W J, Yi Z, Sun L-H and Yan Y 2018 *J. Opt. Soc. Am. B* **35** 652
- [7] Zhang J S and Chen A-X 2018 *arxiv* 1810.13052
- [8] Hossein-Zadeh M and Vahala K J 2007 *Opt. Lett.* **32** 1611
- [9] Huang K and Hossein-Zadeh M 2017 *Opt. Lett.* **42** 1946
- [10] Purdy T P, Yu P-L, Kampel N S, Peterson R W, Cicak K, Simmonds R W and Regal C A 2015 *Phys. Rev. A* **92** 031802(R)
- [11] Purdy T P, Grutter K E, Srinivasan K and Taylor J M 2017 *Science* **356** 1265
- [12] Marquardt F, Chen J P, Clerk A A and Girvin S M 2007 *Phys. Rev. Lett.* **99** 093902
- [13] Wilson-Rae I, Nooshi N, Zwerger W and Kippenberg T J 2007 *Phys. Rev. Lett.* **99** 093901
- [14] Khorasani S 2018 *Sci. Rep.* **8** 11566
- [15] Khorasani S 2017 *Appl. Sci.* **7** 656

- [16] Khorasani S *Photonics* **4** 48
- [17] Khorasani S 2018 *Sci. Rep.* **8** 16676
- [18] Khorasani S 2019 *arxiv* 1804.07053 (accepted)
- [19] Khorasani S 2018 *Quantum Mechanics: Theory, Analysis and Applications* (Arbab A I, ed, Nova Science Publishers, New York) Chap. 1
- [20] Khorasani S and Cabon B 2009 *Scientia Iranica* **16** 157
- [21] Rakich P and Marquardt F 2018 *New J. Phys.* **20** 045005
- [22] Dresselhaus M S, Dresselhaus G, and Eklund P C 1996 *J. Raman Spect.* **27** 351
- [23] Souza Filho A G, Chou S G, Samsonidze G G, Dresselhaus G, Dresselhaus M S, An L, Liu J, Swan A K, Ünlü M S, Goldberg B B, Jorio A, Grüneis A and Saito R 2004 *Phys. Rev. B* **69** 115428
- [24] Dresselhaus M S, Dresselhaus G, Saito R and Jorio A 2005 *Phys. Rep.* **409** 47
- [25] Tan, P-H ed 2019 *Raman Spectroscopy of Two-dimensional Materials* (Springer, Singapore)
- [26] Shao, F and Zenobi, R 2019 *Anal. Bioanal. Chem.* **411** 37
- [27] Khorasani S 2018 *Commun. Theor. Phys.* **70** 334
- [28] Goldstein T, Chen S-Y, Tong J, Xiao D, Ramasubramanian A and Yan J 2016 *Sci. Rep.* **6** 28024
- [29] Zhang X, Qiao X-F, Shi W, Wu J-B, Jiang D-S and Tan P-H 2015 *Chem. Soc. Rev.* **44** 2757
- [30] Tuschel D 2015 *Spectroscopy* **30** 18
- [31] Saito R, Hofmann M, Dresselhaus G, Jorio A and Dresselhaus M S 2011 *Adv. Phys.* **60** 413
- [32] Wu J-B, Lin M-L, Cong X, Liua H-N and Tan P-H 2018 *Chem. Soc. Rev.* **47** 1822
- [33] <https://www.nanophoton.net/raman/raman-spectroscopy.html>
- [34] Benz F, Schmidt M K, Dreismann A, Chikkaraddy R, Zhang Y, Demetriadou A, Carnegie C, Ohadi H, de Nijs B, Esteban R, Aizpurua J and Baumberg J J 2016 *Science* **354** 726
- [35] Benz F, Schmidt M K, Dreismann A, Chikkaraddy R, Zhang Y, Demetriadou A, Carnegie C, Ohadi H, de Nijs B, Esteban R, Aizpurua J and Baumberg J J 2016 [Data set] *Apollo* doi:10.17863/CAM.1675
- [36] Runcorn T H, Murray R T and Taylor J R 2018 *Opt. Express* **26** 4440
- [37] Runcorn T H, Murray R T and Taylor J R 2018 [Data set] *Zenodo* doi:10.5281/zenodo.1166082
- [38] Di Stefano O, Settineri A, Macrì V, Ridolfo A, Stassi R, Kockum A F, Savasta S and Nori F 2017 *arxiv* 1712.00121
- [39] Jansen E, Machado J D P and Blanter Y M 2018 *arxiv* 1811.01605
- [40] Capmany J and Fernández-Pousa C R 2010 *J. Opt. Soc. Am. B* **27** A119
- [41] Schmidt M K, Esteban R, González-Tudela A, Giedke G and Aizpurua J 2016 *ACS Nano* **10** 6291
- [42] Lombardi A, Schmidt M K, Weller L, Deacon W M, Benz F, de Nijs B, Aizpurua J and Baumberg J J 2018 *Phys. Rev. X* **8** 011016
- [43] Roelli P, Galland C, Piro N and Kippenberg T J 2016 *Nature Nanotech.* **11** 164